J. Fluid Mech. (1990), *vol.* 212, *pp.* 55–63
Printed in Great Britain

Dynamics of wetting: local contact angles

By P. G. DE GENNES, X. HUA AND P. LEVINSON
Collège de France, F-75231 Paris Cedex 05, France

(Received 30 June 1989)

We discuss the motion of a triple line for a fluid spreading on a flat solid surface in conditions of partial wetting: the equilibrium contact angle θ_e is assumed to be finite but small: $0 < \theta_e \ll 1$. We distinguish four regions: (1) a molecular domain of size a ($\approx$ a few Ångströms) very near the triple line, where the continuum description breaks down; (2) a proximal region (of length a/θ_e^2 and height a/θ_e) where the long-range Van der Waals forces dominate; (3) a central region, where capillary forces and Poiseuille friction are the only important ingredients; (4) a distal region where macroscopic features (related to the size of the droplet, or to gravitational forces) come into play. In regions (2, 3, 4) the flow may be described in a lubrication approximation, and with a linearized form of the capillary forces. We restrict our attention to low capillary numbers Ca and expand the profiles to first order in Ca near the static solution. The main results are: (*a*) the logarithmic singularity which would have occurred in a simple wedge picture is truncated by the long-range forces, at a fluid thickness a/θ_e. This effect is more important, at small θ_e, than the effects of slippage which have often been proposed to remove the singularity, and which would lead to a truncation thickness comparable with the molecular size a; (*b*) in the central region, the local slope $\theta(x)$ grows logarithmically with the distance x from the triple line; (*c*) one can match explicitly the solutions in the central and distal region: we do this for one specific example: a plate plunging into a fluid with an incidence angle exactly equal to θ_e. In this case we show that, far inside the distal region, the perturbation of the slope decays like $1/x^2$.

1. Introduction

The dynamics of a moving contact line is important for many practical processes, but is complex: see for instance Dussan V. (1979). Some time ago, Huh & Scriven (1971) considered the case of a simple fluid wedge (figure 1*a*) and showed that the wedge profile leads to a logarithmic singularity in the viscous dissipation. Many experiments have been conducted on moving contact lines: in particular the early results of Hoffmann (1975), Tanner (1979), and Lelah & Marmur (1981) show that, for simple liquids, on a completely wettable surface, the relation between line velocity U and dynamic contact angle θ is essentially of the form

$$Ca = \frac{\eta U}{\gamma} = \text{const.}\,\theta^3 \quad (\theta \ll 1), \tag{1}$$

where η and γ are the viscosity and the surface tension of the liquid. This relation is amazingly universal: it does not depend on the value of the spreading coefficient

$$S = \gamma_{SO} - \gamma_{SL} - \gamma \quad (S > 0) \tag{2}$$

(where γ_{SO} and γ_{SL} are the solid/air and solid/liquid interfacial energies). S measures

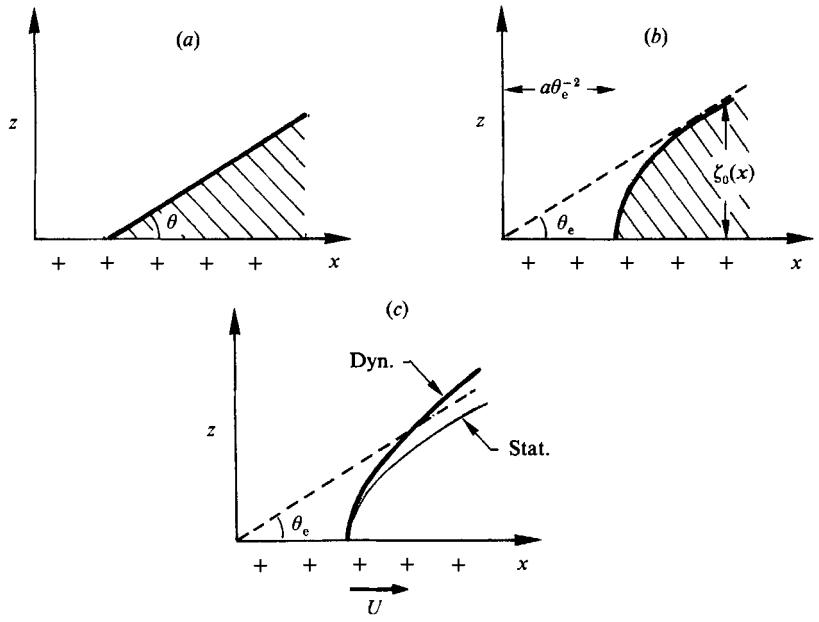

FIGURE 1. Fluid profiles near a contact line, in conditions of partial wetting. (*a*) The simple wedge model, leading to a logarithmic singularity in the dissipation. (*b*) After inclusion of a long-range Van der Waals force, the static profile is hyperbolic. (*c*) Imposing a small flow velocity U shifts the profile as shown. All the analysis in the text is restricted to the case of small equilibrium angles θ_e.

the driving force of the process, but U does not depend on S: this can be understood in terms of the precursor film, first observed by Hardy (1919). All the free energy S is burnt in the precursor film. The θ^3 factor in the Hoffmann–Tanner law (equation (1)) can then be understood as a superposition of a driving force $\gamma(1-\cos\theta) \approx \frac{1}{2}\gamma\theta^2$ and a Huh–Scriven friction factor, essentially linear in θ (de Gennes 1985). The same type of analysis can be applied to conditions of partial wetting, where $S < 0$, and where there exists a finite equilibrium angle θ_e. In these conditions, there is no precursor film (Hardy 1919) and the driving force is the uncompensated Young force $\gamma(\cos\theta_e - \cos\theta)$. This leads to (de Gennes 1986)

$$U = \text{const.}\frac{\gamma}{\eta}\theta(\theta_e^2 - \theta^2) \quad (\theta_e, \theta \ll 1). \tag{3}$$

However, this simple picture leaves some open questions:

(*a*) certain logarithmic prefactors are treated as numerical constants.

(*b*) What provides the cut off in the logarithmic singularity?

(*c*) The very definition of the dynamic angle θ is delicate: at small distances (< 100 μm) from the contact line, the local slope $\theta(x)$ is still significantly dependent on x, as shown by Ngan & Dussan V. (1982), and in more recent experiments by Dussan V. (to be published).

The main aim of the present work is to discuss the local slopes $\theta(x)$, and the dominant physical cut-off for the line singularity. The standard procedure used in the past to remove the singularity was based on slippage at the solid/fluid interface (Hocking 1977; Hocking & Rivers 1982). Instead of the standard boundary condition $v_x(z = 0) = 0$ at a fixed surface, a mixed condition is imposed:

$$b\frac{\partial v_x}{\partial z} = v_x, \quad \text{at} \quad z = 0$$

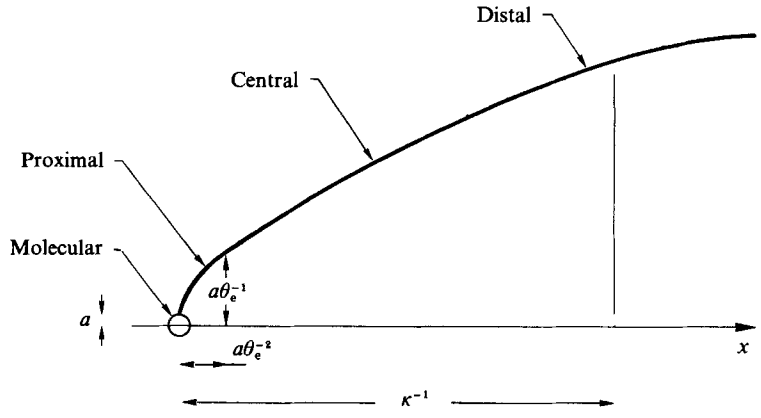

FIGURE 2. The four regions in the profile: (1) molecular; (2) proximal (controlled by long range forces); (3) central (controlled by shear flow plus capillarity); (4) distal (controlled by shear flow plus gravitational forces).

(where z is the normal to the interface). In most usual situations, the slippage length, b, should be comparable with a molecular size a†. The effect of the mixed boundary condition is to suppress the singularity at wedge thicknesses smaller than b (or at distances x smaller than b/θ). At distances $x \gg b/\theta$, the liquid profile becomes universal – as pointed out in particular by Dussan V. (1976) – and depends only weakly (logarithmically) on the choice of b.

The most detailed calculations of this type have been performed by Cox (1986). They ultimately lead to an equation of motion similar to (3), but extended to large angles ($\theta, \theta_e \approx 1$). This equation of motion has been tested in recent measurements by Fermigier (1989), using a photographic measurement of θ inside a capillary where the fluid is pushed at velocity U by a piston. The Cox predictions work very well: this shows that most of the dissipation near the moving contact line can be described in terms of macroscopic viscous friction. But it does *not* prove that slippage is the major physical effect – other processes, leading to different cut-offs near the line, would give the same level of agreement.

The slippage process certainly exists, but it is only relevant for a thickness $b \approx a$, i.e. precisely in the regime where the whole continuum description breaks down: when the dynamic contact angle θ is large ($\theta \approx 1$), there is no characteristic length, other than a, to control the inner structure of the triple line. However, as we shall see (and as already announced by de Gennes 1985), the situation is improved if we deal with small angles $\theta \ll 1$. Here, the relevant thickness turns out to be $a/\theta \gg a$, and a continuum description may be applied to find the correct cut-off in the singularity, which is due to long-range Van der Waals forces, and not to slippage.

We shall concentrate here on the situation of partial wetting, without any precursor film: this leads to a relatively simple problem; but even so, we shall need to distinguish four spatial regions around the contact line: molecular, proximal, central and distal (figure 2). Our method starts from the exact static shapes, including long-range Van der Waals forces (§2). Then, in §3 we treat the velocity U as a perturbation, and find the first-order corrections to the static profile in the

† There may exist exceptional cases where $b \gg a$ – for instance with a flow of entangled polymers along a passive wall, see de Gennes (1979). But this type of flow has not been demonstrated in the usual model system (silicone oil against silica).

'proximal' and 'central' regions. Finally, in §4 we show how to match these results with the meniscus, or 'distal' profile, controlled in many examples by gravitational forces.

A final introductory remark concerns orders of magnitude. Equation (3) shows that, in retraction ($\theta < \theta_e$), a contact line can exist only for velocities U below a certain threshold

$$U_{max} = \text{const.} \frac{\gamma \theta_e^3}{\eta}.$$

At $U > U_{max}$ the retracting liquid leaves a permanent film on the solid. All the discussions in the following sections assume that θ is close to θ_e, or equivalently that $U < U_{max}$. Taking $\theta_e = 1°$, $\gamma = 50$ c.g.s. units, and $\eta = 10^{-2}$ P, we find $U_{max} \approx \frac{1}{4}$ mm/s. Thus we are talking about low velocities, which are indeed most suitable for precise optical measurements on the profiles.

2. Proximal and central regions

2.1. *Basic flow equation*

In a reference frame attached to the triple line (figure 1*b*), we expect a fluid thickness $\zeta(x)$ which will incorporate the effects of capillarity, of long-range forces (described by a Hamaker constant A) and of slow Poiseuille flows. We always restrict our attention to situations of small slopes:

$$\left|\frac{\partial \zeta}{\partial x}\right| \ll 1.$$

This will allow three simplifications: (*a*) a linearized form for the capillary pressure $-\gamma \partial^2 \zeta / \partial x^2$; (*b*) a lubrication approximation for the flow; (*c*) a simple description of the Van der Waals forces. The basic equation is then (de Gennes 1985):

$$\frac{3\eta U}{\zeta^2} = \frac{A}{2\pi \zeta^4} \frac{\mathrm{d}\zeta}{\mathrm{d}x} - \gamma \frac{\mathrm{d}^3 \zeta}{\mathrm{d}x^3}. \tag{4}$$

The left-hand side represents Poiseuille friction. The first term on the right-hand side is the gradient of the disjoining pressure Π due to long-range Van der Waals forces,

$$\Pi = \frac{A}{6\pi \zeta^3}. \tag{5}$$

It is convenent to introduce a length a:

$$a^2 = \frac{A}{6\pi\gamma} \tag{6}$$

(a is of the order of a molecular size: a few Ångströms). Introducing dimensionless variables

$$z = \frac{\theta_e}{a} \zeta, \quad y = \frac{\theta_e^2}{a} x$$

and a perturbation parameter

$$\epsilon = \frac{3U\eta}{\gamma \theta_e^3} = \frac{3Ca}{\theta_e^3} \tag{7}$$

we can cast (4) into the form

$$\epsilon = \frac{3}{z^2} z' - z^2 z''', \tag{8}$$

where $z' = \mathrm{d}z/\mathrm{d}y$, etc.

2.2. *The static limit*

For $\epsilon = 0$, equation (8) may be integrated exactly (Berry 1974) and the result is

$$z_0^2 = -1 + y^2 \tag{9}$$

The profile is hyperbolic (figure 1*b*). The slope $\mathrm{d}\zeta/\mathrm{d}x$ deviates from its macroscopic value (θ_e) at thicknesses $\zeta \approx a/\theta_e$ (corresponding to $z_0 < 1$). It is important to check that (9) gives slopes $\mathrm{d}\zeta/\mathrm{d}x$ that are small, so that the approximations (*a*, *b*, *c*) listed in §2.1 do apply. Indeed, we find

$$\frac{\mathrm{d}\zeta_0}{\mathrm{d}x} = \theta_e z_0' = \theta_e \frac{y}{z_0}. \tag{10}$$

Even in the most dangerous region ($y \to 1$), we have $\mathrm{d}\zeta/\mathrm{d}x \approx \theta_e/z_0 \approx \theta_e a/\zeta$ and the slope becomes large only when we go down to $\zeta \approx a$, i.e. when we enter the molecular domain.

3. First-order calculation of the proximal and central profiles

We now return to (8) and treat the ϵ term (describing the effects of the line velocity, figure 1*c*) as a perturbation, following a method used by Joanny (1984) in a similar problem. We define

$$F = \tfrac{1}{2}z'^2 - \tfrac{1}{2}z'^{-2}. \tag{11}$$

In the static case ($\epsilon = 0$), F is a constant. In the dynamic case ($\epsilon \neq 0$), F is variable: we consider F as a function of y, when $z(y)$ is the steady-state profile. We can then show (using (8)) that

$$\frac{\mathrm{d}F}{\mathrm{d}y} = \frac{\epsilon}{z(y)}. \tag{12}$$

It is then easy to compute F to first order in ϵ:

$$F = \tfrac{1}{2} + \epsilon \int_0^y \frac{\mathrm{d}u}{z_0(u)}, \tag{13}$$

where z_0 is the static solution, (9). The integral in (13) can be performed by setting $u = \sinh t$, and the result is

$$F = \tfrac{1}{2} + \epsilon \operatorname{Arg\,sinh} y. \tag{14}$$

Let us now focus our attention on the region $y \gg 1$, where the effect of the long-range forces has become negligible, and $F \to \frac{1}{2}z'^2$. Here, using (11) and (14), we arrive at a local slope

$$\frac{\mathrm{d}\zeta}{\mathrm{d}x} = \theta = \theta_e \frac{\mathrm{d}z}{\mathrm{d}y} = \theta_e \left[1 + \epsilon \ln\left(\frac{2x\theta_e^2}{a}\right)\right]. \tag{15}$$

Equation (15) is our central result. The logarithmic behaviour of $\theta - \theta_e$ is not a surprise, and has been found in all slippage models. But the characteristic length $\Delta x \approx a/\theta_e^2$ showing up in the logarithm is non-trivial: the long-range forces provide a natural cut-off for the singularity at fluid thicknesses $\Delta\zeta \approx \theta_e \Delta x \approx a/\theta_e$. This cut-off dominates over slippage effects which lead to $\Delta\zeta_{\mathrm{slip}} \approx a$ (a molecular size).

It may also be worthwhile to emphasize the physical meaning of the function F: this can be done by an inspection of the dissipation $T\Sigma$ (per unit length of line) between the line ($x = x_L$) and point (x):

$$T\Sigma = \int_{x_L}^{x} 3\eta \frac{U^2}{\zeta} \mathrm{d}x. \tag{16}$$

To second order in U, we may replace $\zeta(x)$ by the static profile, obtaining

$$T\Sigma \frac{3\eta U^2}{\theta_e} \int_1^y \frac{du}{z_0(u)}. \tag{17}$$

The integral in (17) may be expressed in terms of the F-function via (13). In the central region ($u \gg 1$), F is related to the local slope θ via (11):

$$2F - 1 = \theta^2/\theta_e^2 - 1 \approx (\cos\theta_e - \cos\theta)\, 2/\theta_e^2. \tag{18}$$

Inserting this into (17), we arrive at

$$T\Sigma = U\gamma(\cos\theta_e - \cos\theta). \tag{19}$$

Equation (16) expresses the dissipation as the product of a flux (U) and a non-compensated Young force $\gamma(\cos\theta_e - \cos\theta)$, and could have been written down directly.

4. The meniscus (or distal) region

4.1. *Incorporation of gravity*

The final problem is to match the solution (15) in the central region to an external boundary condition very far from the line. We shall discuss this for a relatively simple, but instructive example, shown on figure 3. Here we have a solid plate inclined exactly at the angle θ_e, and we move this plate in its own plane, at a velocity U. For $U = 0$, the liquid was horizontal everywhere. But for a finite $U > 0$, we expect a dip in the liquid surface.

Incorporating the gravitational forces ρg (where ρ is the fluid density) and dropping the long-range forces, we arrive at a modified equation for the profiles ($\theta_e \ll 1$):

$$\frac{3\eta U}{\zeta^2} = -\gamma \frac{d^3\zeta}{dx^3} + \rho g\left(\frac{d\zeta}{dx} - \theta_e\right). \tag{20}$$

We define a capillary length κ^{-1} via

$$\kappa^2 = \frac{\rho g}{\gamma}, \tag{21}$$

and a dimensionless number

$$\mu = \frac{\kappa a}{\theta_e^2}. \tag{22}$$

Typically $\mu \approx 10^{-6}$. Retaining our former definitions of z and y, we can cast (20) into the form

$$\frac{\epsilon}{z^2} = -z''' + \mu^2(z' - 1). \tag{23}$$

It is convenient to separate the dynamic correction v to the profile:

$$\frac{dz}{dy} = 1 + v(y). \tag{24}$$

To first order in ϵ we may replace z by y in the left-hand side of (23). This gives

$$v'' - \mu^2 v = -\frac{\epsilon}{y^2}. \tag{25}$$

Note that we have shifted the origin to the actual position of the triple line (point I in figure 3). The boundary conditions are

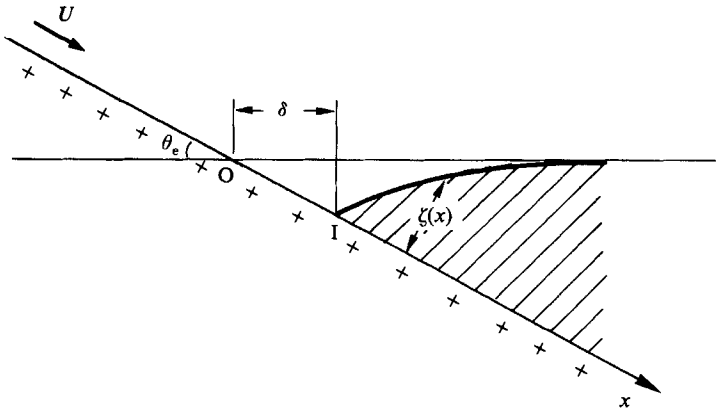

FIGURE 3. A specific example: plate plunging exactly at the equilibrium angle θ_e. In static conditions, the fluid is a simple wedge. When the plate moves at velocity U, the contact line is shifted by a length δ, and a perturbed region extends up to the capillary length κ^{-1}.

(*a*) for $\mu y \ll 1$ (matching to the central region), we must follow (15):

$$v(y \to 0) \to \epsilon \ln(2y); \tag{26}$$

(*b*) for $\mu y \gg 1$, the fluid must return to a horizontal slope

$$v(y \to +\infty) \to 0.$$

4.2. *Solution*

It is sometimes convenient to separate from v the term (which we shall call ϵQ) that is obtained in the absence of gravity:

$$v = \epsilon Q + w. \tag{27}$$

We know from (15) that, in the central region,

$$Q = \ln(2y). \tag{28}$$

The equation for w deduced from (26) is

$$w'' - \mu^2 \omega = \epsilon \mu^2 Q \tag{29}$$

and a general solution is of the form

$$w/\epsilon = k\,\mathrm{e}^{-\mu y} + k'\,\mathrm{e}^{\mu y} - \int_0^\infty \mathrm{d}m\, G(y-m)\, Q(m), \tag{30}$$

when the first two terms are solutions of the homogeneous equation ($Q = 0$) while the third term is one particular solution of (26). Here

$$G(y-m) = \tfrac{1}{2}\mu\,\mathrm{e}^{-(\mu|y-m|)}. \tag{31}$$

The boundary condition at $y \to \infty$ immediately gives $k' = 0$, while the boundary condition at $y = 0$ imposes

$$k - \int_0^\infty \mathrm{d}m\, \tfrac{1}{2}\mu\,\mathrm{e}^{-\mu m} \ln(2m) = 0, \tag{32}$$

or

$$k = \tfrac{1}{2}\ln\left(\frac{2}{\mu\tilde{\gamma}}\right), \tag{33}$$

where $\tilde{\gamma} = 1.78$ is Euler's constant.

The aspect of the solution $v(y)$ is shown on figure 3. At large distances ($\mu y > 1$), one can see immediately from (25) that v decreases only slowly:

$$v = \frac{\epsilon}{(\mu y)^2} \quad (\mu y > 1). \tag{34}$$

Equation (34) expresses a simple balance between shear stresses and gravitational pressures.

One interesting observable is the shift $\delta \approx \mathrm{OI}$ in the position of the contact line, due to the motion. Returning to figure 3, we see that

$$\theta_e \delta = \int_0^\infty \frac{\mathrm{d}}{\mathrm{d}x}(\zeta - \zeta_0)\,\mathrm{d}x = \frac{a}{\theta_e}\int_0^\infty v\,\mathrm{d}y. \tag{35}$$

Integrating (25) over y, we get

$$\mu^2 \int_y^\infty v\,\mathrm{d}y = \frac{\epsilon}{y} - v'(y) = \frac{\epsilon}{y} - \epsilon Q' - w', \tag{36}$$

and finally

$$\mu^2 \int_0^\infty v\,\mathrm{d}y = -w'(0) = 2\mu k\epsilon, \tag{37}$$

the last form being obtained after explicit differentiation of G in (30).

Inserting (37) into (35), and making use of (33) for k, we arrive at

$$\delta = \epsilon\kappa^{-1} \ln\left(\frac{2}{\mu\tilde{\gamma}}\right). \tag{38}$$

Typically, $\delta \approx 15\epsilon\kappa^{-1}$.

5. Concluding remarks

We have constructed the liquid profile in all three regions where continuum mechanics may be applied: proximal, central and meniscus. Of particular interest is the result for the central region (equation (15)) which shows precisely how the existence of long-range Van der Waals forces suppresses the singularity at the contact line. Of course it may happen that dissipation processes in the proximal region – i.e. at the molecular scale – play a role: however, if the local viscosity at these small scales is not much higher than the bulk viscosity η, we can see that the proximal region is not important.

Equation (15) may be of some practical use in discussing experiments where the local slope $\theta(x)$ is measured optically. Unfortunately, the data of Ngan & Dussan V. (1982) are taken for a solid which is probably completely wetted ($\theta_e^2 < 0$) and thus do not correspond exactly to our problem. But, for conditions of partial wetting, with ideally flat surfaces (no hysteresis), (15) should be applicable.

A final remark concerns the dissipation: with the example described in figure 3, we get convergent answers for the meniscus shape. However, the dissipation itself remains divergent at large scales. To order U^2, it is always given by (17), or explicitly by

$$T\Sigma = \frac{3\eta U^2}{\theta_e} \ln\left[\frac{2x_{\max}\theta_e^2}{a}\right], \tag{39}$$

and it does depend on the horizontal size of the basin (defined in (36) by $x_{\max}$). This is an intrinsic feature of the wedge geometry which is imposed in figure 3.

Our analysis was strictly restricted to situations of partial wetting. In conditions of complete wetting, the discussion is more complex, because it must include the precursor film. The existence of the precursor depends on Van der Waals forces (or other long-range forces): thus it is obvious that, in this situation too, triple-line motions cannot be discussed without due incorporation of the long-range forces.

When the spreading coefficient S is large ($S/\gamma \approx 1$), the precursor is of molecular thickness, and its tip cannot be described by hydrodynamic theories. But when $S/\gamma \ll 1$, the precursor is relatively thick, and continuum theory applies. In this case, near the tip, the static shape is also a good starting point, as shown by Joanny (1984).

This work was initiated by a seminar of E. Dussan V. at Exxon Corporate Research in October 1988. Discussions with J.-F. Joanny and F. Brochard have also been of great help.

REFERENCES

BERRY, M. 1974 *J. Phys.* A **7**, 231.

COX, R. G. 1966 *J. Fluid Mech.* **168**, 169.

DUSSAN V., E. B. 1979 *Ann. Rev. Fluid Mech.* **11**, 371–400.

DUSSAN V., E. B. 1976 *J. Fluid Mech.* **77**, 665.

FERMIGIER, M. 1989 Dynamique d'une interface liquide dans un capillaire. Thèse, Université Paris 6.

GENNES, P. G. DE 1979 *C.R. Acad. Sci. Paris* B **288**, 219.

GENNES, P. G. DE 1985 *Rev. Mod. Phys.* **57**, 827.

GENNES, P. G. DE 1986 *Z. Kolloid Polymer Sci.* **264**, 463.

HARDY, W. 1919 *Phil. Mag.* **38**, 49.

HOCKING, L. M. 1977 *J. Fluid Mech.* **79**, 209.

HOCKING, L. M. & RIVERS, A. 1982 *J. Fluid Mech.* **121**, 425.

HOFFMANN, R. 1975 *J. Colloid Interface Sci.* **50**, 228.

HUH, C. & SCRIVEN, L. E. 1971 *J. Colloid Interface Sci.* **35**, 85.

JOANNY, J.-F. 1984 Le mouillage. Thèse, Paris.

LELAH, M. & MARMUR, A. 1981 *J. Colloid Interface Sci.* **82**, 518.

NGAN, C. & DUSSAN V., E. B. 1982 *J. Fluid Mech.* **118**, 27.

TANNER, L. 1979 *J. Phys.* D **12**, 1473.

TELETZKE, G. F., DAVIES, H. T., SCRIVEN, L. E. 1988 *Rev. Phys. Appl.* **23**, 989.